Prediction and Validation of Whirl Flutter Data of the Maryland Tiltrotor Rig

Seyhan Gul*
Graduate Research Assistant

Anubhav Datta
Associate Professor

University of Maryland, College Park, MD

University of Maryland's Maryland Tiltrotor Rig was tested in the Naval Surface Warfare Center Carderock Division 8-×10-ft subsonic wind tunnel. Flutter frequency and damping data were collected for wing beam and chord modes up to 100 kt. Eight configurations were tested. Baseline data are gimbal-free, freewheeling mode, wing fairings on with straight and swept-tip blades. Gimbal-locked, powered mode, and wing fairings off data were also collected, all with straight and swept-tip blades. The sweep angle is 20°, starting at 80%R. Details of the mathematical model are reported. Predictions were carried out for each configuration with the University of Maryland's new aeromechanics solver UMARC-II. Wing beam damping showed good agreement with the test data. Wing chord damping was underpredicted with a maximum of 0.9% difference. The trends for this mode for the gimbal-locked, straight blades configurations (freewheeling and powered) were not captured by the analysis. Swept-tip blades did not show a definitive increase in wing beam or chord damping for the gimbal-free configuration. However, wing chord damping increased (about 0.4% at 60 kt) due to swept-tip blades for the gimbal-locked, freewheeling configuration. Locking the gimbal increased the wing chord damping by 0.5%, which was picked up by the analysis. Powered mode also increased the wing chord damping by 0.5% compared to freewheeling mode, but the analysis did not predict this behavior. Wing beam damping test data showed an increase at higher speeds due to wing aerodynamics, although not as clearly as predictions due to scatter.

Introduction

The first whirl flutter test of the Maryland Tiltrotor Rig (MTR) was recently completed in the Naval Surface Warfare Center Carderock Division (NSWCCD) 8-×10-ft subsonic wind tunnel. Eight configurations were tested. These are gimbal-free and gimbal-locked, freewheeling and powered modes, wing fairings on and off, and straight and swept-tip blades. Two sets of straight blades and one set of swept-tip blades were tested. An overview of the test is reported in Ref. 1. The details of the swept-tip blades are reported in Ref. 2. This paper focuses on prediction and validation.

The MTR is a new tiltrotor testbed at the University of Maryland (UMD) developed over the last 6 years. The rig is an optionally powered, hub interchangeable, semispan tiltrotor meant for testing proprotors up to 4.75-ft (1.45-m) diameter in the Glenn L. Martin wind tunnel (7.75-×11-ft test section with 200 kt maximum speed). The objective of this facility is to provide a testbed for basic research on aeromechanics of high-speed tiltrotors. The detailed design and construction of the rig was carried out by Calspan Corporation. The composite blades and wing spars were designed and fabricated in-house at the UMD. The design, fabrication, and instrumentation are reported in detail in Refs. 1, 3, and 4. The design analysis for the hingeless hub is reported in Ref. 5. The design and fabrication of the blades are described in Ref. 6 for the straight blades and in Ref. 7 for the swept-tip blades.

There has been important analytical work on the high-speed stability of proprotors, given in Refs. 8–30 in chronological order. Most of these focused on XV-15/V-22-like configurations. MTR is a new research test facility not strictly representative of any legacy rotor. Together with MTR, a new aeromechanics solver was developed at the UMD to study the stability mechanisms from first principles. The solver was named UMARC-II. UMARC-II departs from UMARC (Ref. 31) with its numerical extraction of aerodynamic and inertial terms which eliminates small term assumptions, its generic fixed-rotating interface, and multibody joint modeling. A lot of these features are also available in commercial codes, but the pursuit of fundamental understanding of the problem at hand and dissection of its principal mechanisms favored the development of a new solver. Theory for the key features and validation are reported in Ref. 32. Historically, validation data were limited (and not available for swept-tip blades at all) up to now. This paper reports a parametric study and validation for this new solver with the recently acquired whirl flutter data.

Maryland Tiltrotor Rig

MTR is an optionally powered semispan rig that supports interchangeable hubs (gimballed and hingeless), blades (straight and swept-tip), and wing spars in order to allow for a systematic variation of components that are important for whirl flutter. The rig consists of the wing

*Corresponding author; email: sgul@umd.edu.

Presented at AIAA SCITECH 2022 Forum, San Diego, CA & Virtual, January 3–7, 2022. Manuscript received February 2022; accepted October 2023.

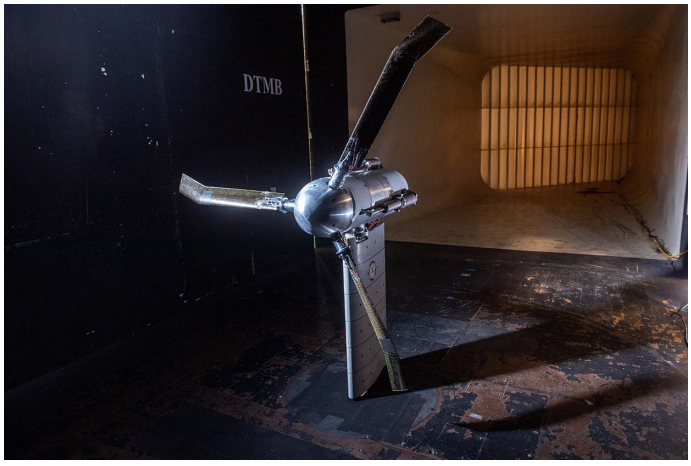

Fig. 1. MTR in the Navy Carderock wind tunnel.

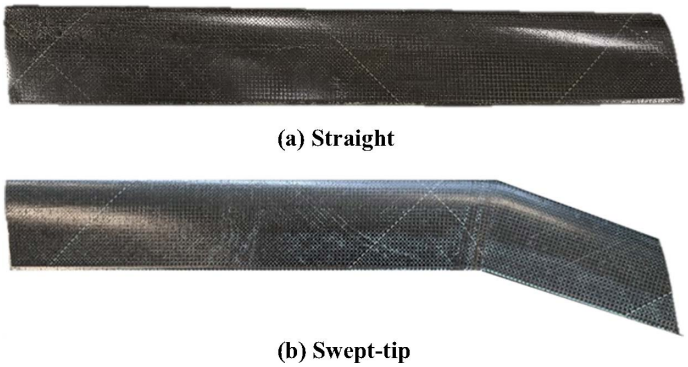

(a) Straight

(b) Swept-tip

Fig. 2. MTR blades.

Table 1. MTR rotor properties

Number of blades	3
Rotor radius	0.724 m (2.375 ft)
Blade chord	0.08 m (3.15 in)
Precone	2°
Pitch flap coupling (δ_3)	−15°
Lock number (γ) for straight blades	2.37
Blade twist	−37°
Rotor speed (Froude-scaled)	1050 rpm
Rotation direction	counterclockwise
Blade airfoil	VR-7 (tab = 0)
Blade root cutout	27%

Table 2. MTR wing/pylon properties

Wing span	0.927 m (3.042 ft)
Wing chord	0.392 m (1.287 ft)
Wing airfoil	NACA 0018
Total wing mass	7.2 kg (15.8 lb)
Mast height	0.243 m (0.8 ft, 33.6%R)
Pylon mass (without rotating components)	28.53 kg (62.9 lb)
Pylon c.g. offset (without rotating components)	0.07 m (2.75 in, 9.7%R) (from elastic axis, toward wing trailing edge)

Table 3. Wing beam mode mass-normalized mode shape

Frequency = 5.1 Hz (0.29/rev)
Structural damping = 0.4%

Point	r (m)	x[a]	y[a]	z[a]	θ_x[b]	θ_y[b]	θ_z[b]
1	0	0	0	0	0	0	0
2	0.0838	0	0	0.0022	−0.0047	−0.0520	0
3	0.2	0	0	0.0121	−0.0111	−0.1157	0
4	0.3	0	0	0.0260	−0.0166	−0.1627	0
5	0.4	0	0	0.0443	−0.0221	−0.2023	0
6	0.5	0	0	0.0663	−0.0276	−0.2348	0
7	0.6	0	0	0.0911	−0.0331	−0.2601	0
8	0.7	0	0	0.1181	−0.0386	−0.2784	0
9	0.7823	0	0	0.1414	−0.0431	−0.2882	0
10	0.9271	0	0	0.1831	−0.0431	−0.2882	0
11	1.1705	0	0	0.1727	−0.0431	−0.2882	0

[a]Unit: $\mathrm{m}/\sqrt{\mathrm{kg\,m^2.}}$
[b]Unit: $\mathrm{rad}/\sqrt{\mathrm{kg\,m^2.}}$

Table 4. Wing chord mode mass-normalized mode shape

Frequency = 9.7 Hz (0.55/rev)
Structural damping = 0.57% (wing fairings on)
= 0.36% (wing fairings off)

Point	r (m)	x[a]	y[a]	z[a]	θ_x[b]	θ_y[b]	θ_z[b]
1	0	0	0	0	0	0	0
2	0.0838	0	0.0021	0	0	0	0.0491
3	0.2	0	0.0114	0	0	0	0.1098
4	0.3	0	0.0247	0	0	0	0.1550
5	0.4	0	0.0422	0	0	0	0.1938
6	0.5	0	0.0632	0	0	0	0.2262
7	0.6	0	0.0872	0	0	0	0.2523
8	0.7	0	0.1135	0	0	0	0.2720
9	0.7823	0	0.1364	0	0	0	0.2837
10	0.9271	0	0.1775	0	0	0	0.2837
11	1.1705	−0.0690	0.1775	0	0	0	0.2837

[a]Unit: $\mathrm{m}/\sqrt{\mathrm{kg\,m^2.}}$
[b]Unit: $\mathrm{rad}/\sqrt{\mathrm{kg\,m^2.}}$

Table 5. Wing torsion mode mass-normalized mode shape

Frequency = 14.4 Hz (0.82/rev)
Structural damping = 2%

Point	r (m)	x[a]	y[a]	z[a]	θ_x[b]	θ_y[b]	θ_z[b]
1	0	0	0	0	0	0	0
2	0.0838	0	0	−0.0010	−0.1105	0.0233	0
3	0.2	0	0	−0.0054	−0.2633	0.0509	0
4	0.3	0	0	−0.0115	−0.3940	0.0704	0
5	0.4	0	0	−0.0193	−0.5234	0.0861	0
6	0.5	0	0	−0.0285	−0.6511	0.0981	0
7	0.6	0	0	−0.0388	−0.7767	0.1068	0
8	0.7	0	0	−0.0498	−0.8999	0.1124	0
9	0.7823	0	0	−0.0592	−0.9991	0.1152	0
10	0.9271	0	0	−0.0759	−0.9991	0.1152	0
11	1.1705	0	0	−0.3190	−0.9991	0.1152	0

[a]Unit: $\mathrm{m}/\sqrt{\mathrm{kg\,m^2.}}$
[b]Unit: $\mathrm{rad}/\sqrt{\mathrm{kg\,m^2.}}$

assembly, motor drive, rotor shaft, hub, swashplate (three-bladed), and instrumentation. The blades and wing spars can be inserted in and out depending on the nature of the investigation. The rig is loosely based on the XV-15 design. The MTR installed in the Navy Carderock wind tunnel is shown in Fig. 1. The blades are shown in Fig. 2. The straight and the swept-tip blades have the same twist. High-level properties of the rig

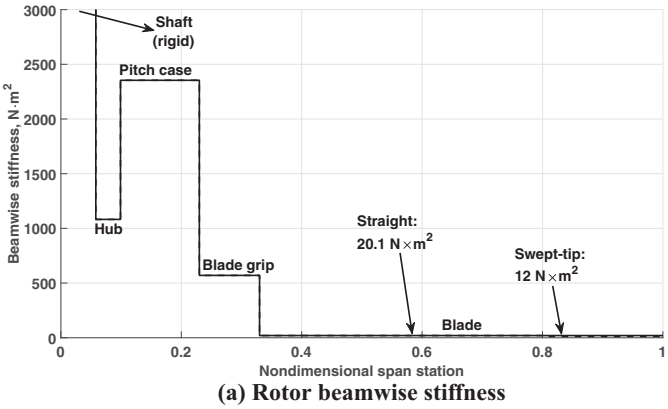

(a) Rotor beamwise stiffness

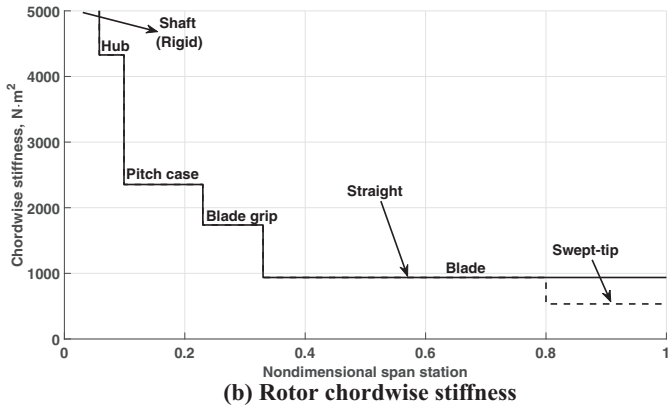

(b) Rotor chordwise stiffness

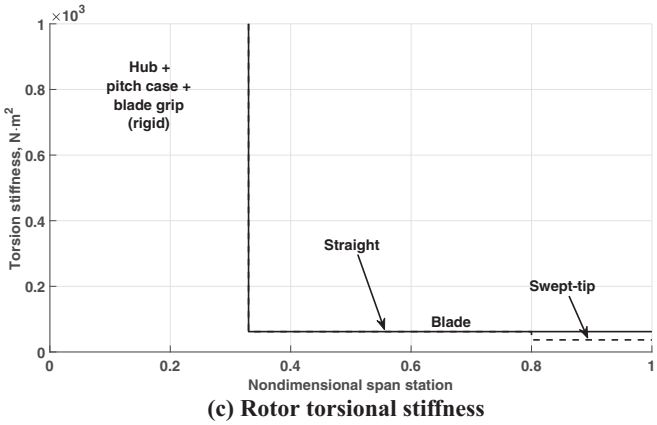

(c) Rotor torsional stiffness

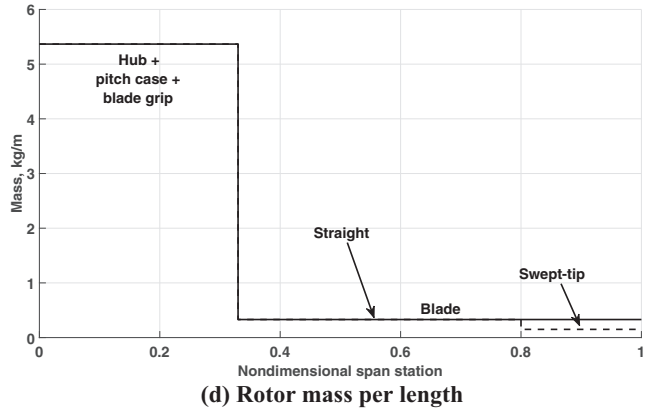

(d) Rotor mass per length

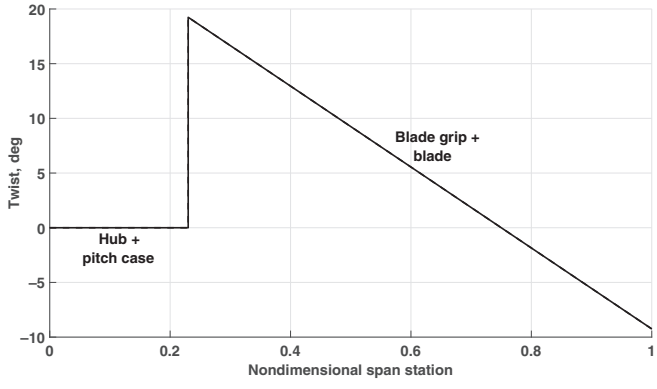

(e) Rotor twist

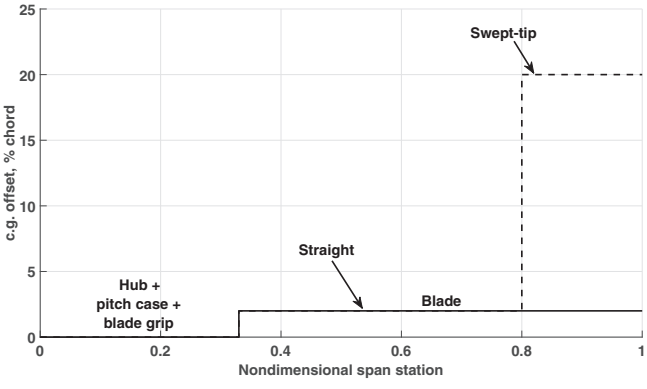

(f) Rotor section c.g. offset from elastic axis (positive toward trailing edge)

Fig. 3. MTR rotor properties.

are given in Tables 1 and 2. Note the high pylon mass in Table 2. This is because the slip ring, swashplate actuators, and electric motor do not follow traditional model scaling laws. The rotor properties are given in Fig. 3. There is no spar at the swept portion of the blade. The section center of gravity (c.g.) is behind the elastic axis even with leading edge weights (Fig. 3f), but this did not create any pitch-flap stability issues due to high torsional stiffness. The wing/pylon properties are reported in Fig. 4. Note that the *x*-axis is the total length from root to point 11 in Fig. 5 along the dashed line. The wing tip is located at 79.2% of the total length (point 10 in Fig. 5), and 100% represents the rotor hub (point 11 in Fig. 5). Mass-normalized mode shapes for wing beam, chord, and torsion modes calculated by UMARC-II are given in Tables 3–5. The nondimensional beam and chord frequencies are typical of full-scale aircraft, except the torsion frequency which is lower due to high pylon mass. The aeromechanics model of the MTR includes a full wing and a pylon; however, the frequencies, mode shapes, and structural damping values are sufficient to model the fixed structure for any future validation study. The structural damping values were measured with rap tests. Note that the chord mode has higher structural damping when the wing fairings are on. The dynamics of the fixed structure are otherwise unaffected by the fairings. The mode shape points and the axis system are shown in Fig. 5.

The UMARC-II model is shown in Fig. 6. The structural model uses long and slender Euler-Bernoulli beams with linear isotropic

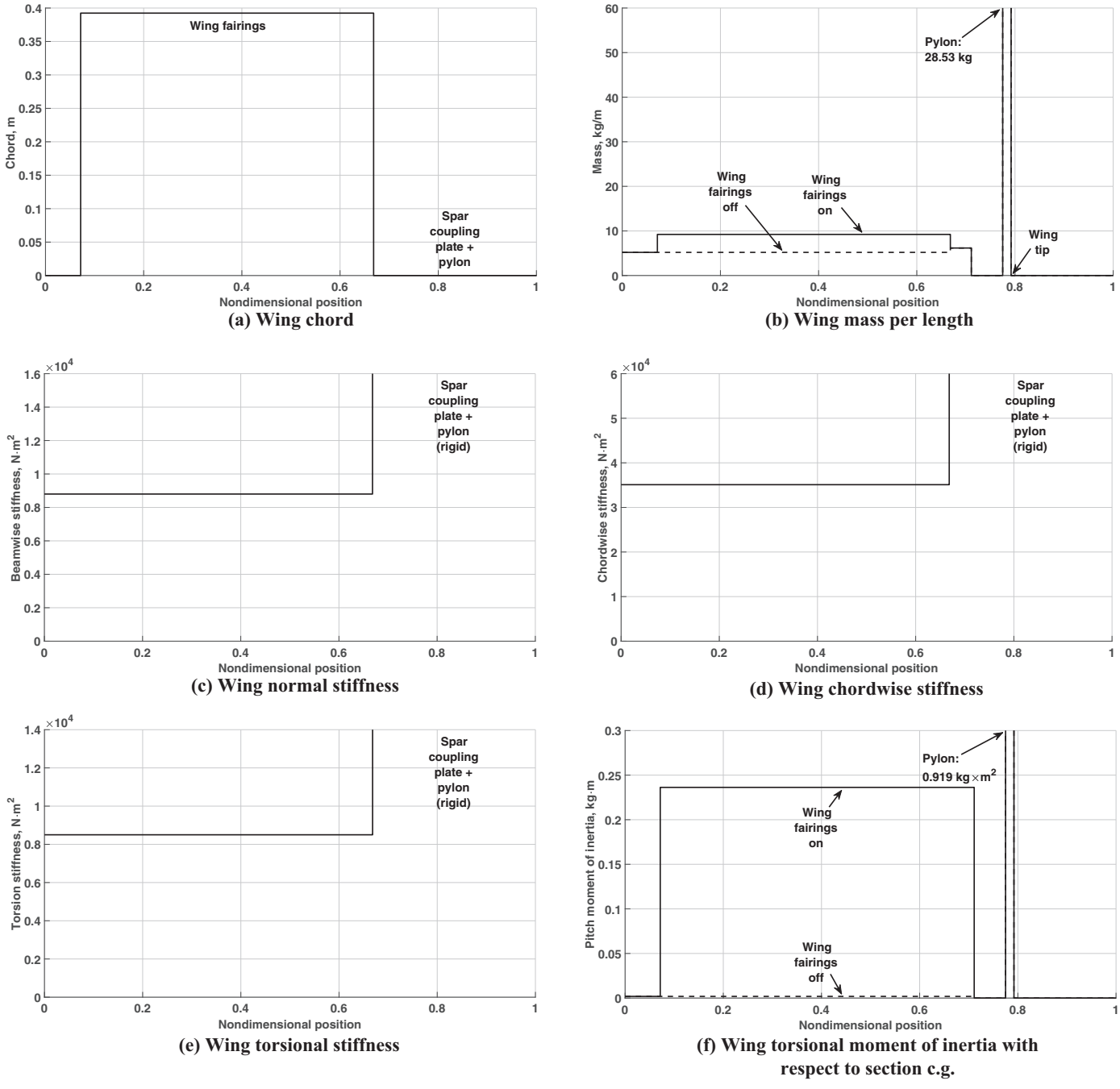

Fig. 4. MTR wing/pylon properties.

materials. The equations of motion were adapted from Hodges and Dowell (Ref. 33). Deformations can be moderate as the model includes nonlinearities up to second order. Blade sweep is modeled by sweeping the elastic axis, which is taken into account with intersegment boundary conditions and elastic axis positions. Aerodynamic and inertial terms are obtained exactly by numerical perturbation with no small term assumption; hence, an ordering scheme is not used. Unsteady lifting-line theory is used. Sectional angles of attack are calculated from flexible blade deformations and hub motions. Large inflow and hub motions important for tiltrotor stability are taken into account exactly.

Fanplots for straight and swept-tip blades are presented in Fig. 7. Both collective and cyclic frequencies are shown. Good agreement with the nonrotating frequency measurements is observed. Swept-tip blades exhibit higher frequencies. This is because of the lower blade mass due to the absence of a spar in the swept region.

Testing Procedure

Flutter frequency and damping data were collected up to 100 kt for wing beam and chord modes. This represents near 230 kt full-scale flight (Froude-scaling for a 25-ft diameter rotor such as the XV-15 aircraft). Higher speeds could not be explored due to a safety restriction from the wind tunnel. Torsion mode frequency and damping were too high to be excited. Baseline data are gimbal-free, freewheeling mode, wing

Table 6. Flutter test conditions

Sweep	Tunnel Speed (kt)	Collective (deg)	Gimbal	Mode	Wing Fairings
Straight blades					
Set 2					
1	30, 40, 50, 60, 65, 70, 74, 78, 82, 86, 89, 92, 96, 100	9.9, 17.6, 22.3, 26.7, 28.2, 30.0, 31.2, 32.8, 34.1, 35.4, 36.8, 37.5, 38.8, 39.8	Free	Freewheel	On
2	30, 40, 50, 60, 65, 70, 74, 78, 82, 86, 89, 92, 96, 100	10.4, 17.3, 22.4, 26.5, 28.6, 30.5, 31.7, 33.4, 34.6, 35.9, 36.8, 37.9, 39.1, 40.1	Free	Freewheel	Off
Set 1					
3	30, 40, 50, 60	11.3, 17.2, 22.1, 26.4	Locked	Freewheel	Off
4	4, 20, 30, 40, 50, 60	3.2, 11.4, 15.8, 20.7, 25.2, 28.9	Locked	Powered	Off
Swept-tip blades					
5	30, 40, 50, 60, 65, 70, 74, 78, 82, 86, 89, 92, 96, 100	13.3, 18.9, 23.5, 27.4, 29.5, 31.2, 32.4, 34.3, 35.2, 37.1, 37.9, 39.0, 39.9, 40.7	Free	Freewheel	On
6	30, 40, 50, 60, 65, 70, 74, 78, 82, 86, 89, 92, 96, 100	11.9, 17.8, 22.0, 26.4 28.8, 30.8, 32.5, 33.8, 35.1, 36.3, 37.8, 38.7, 39.6, 40.6	Free	Freewheel	Off
7	30, 40, 50, 60, 65, 70, 74, 78, 82	11.1, 17.1, 22.1, 26.5, 29.1, 31.4, 32.7, 34.3, 35.1	Locked	Freewheel	Off
8	4, 20, 30, 40, 50, 60	3.4, 13.0, 16.9, 21.6, 25.9, 29.7	Locked	Powered	Off

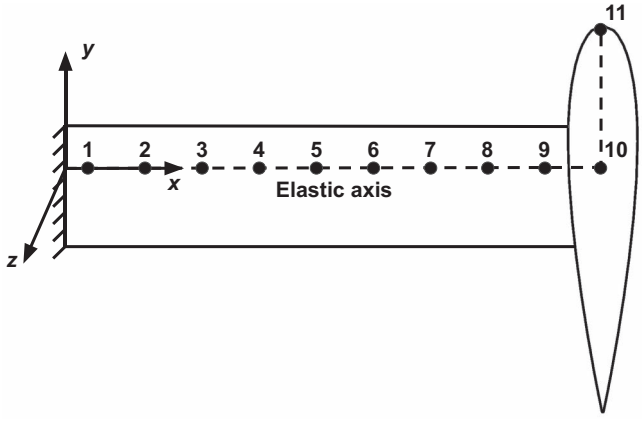

Fig. 5. Mode shape points.

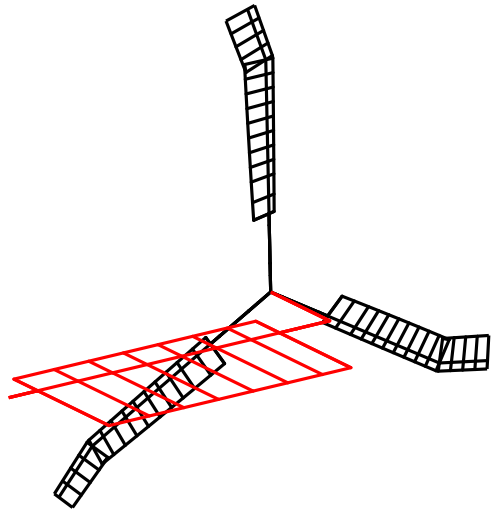

Fig. 6. UMARC-II model of the MTR (rotor, pylon, and wing are beams, panels show aerodynamic segments).

fairings on with straight and swept-tip blades. Gimbal-locked (essentially a hyper-stiff in-plane hingeless hub with a high flap frequency), powered mode, and wing fairings off data were also collected, all with straight (two sets of blades) and swept-tip blades. The sweep angle is 20°, starting at 80%R. The test conditions are shown in Table 6.

The rotor was trimmed to 1050 rpm (Froude-scaled Bell XV-15 rotor speed) at each tunnel speed. Analysis guided the test to find the trim collective. Then, the wing modes were excited with the high-bandwidth swashplate actuators. Wing beam mode was excited by oscillating the longitudinal cyclic at the beam frequency, and the chord mode was excited by oscillating the collective at the chord frequency. After the excitation stopped, the decay in the signal was recorded and the Moving-Block method (Ref. 34) was used to extract the damping value. Analysis also helped here to ensure safety during the stability tests. At least three trials were carried out for each wing mode. A detailed description of the test setup and the testing procedure is given in Ref. 1.

Freewheeling Predictions

Whirl flutter tests are typically conducted at the freewheeling mode because of the conservative stability boundary while achieving near representative collective as powered flight (Ref. 11). Testing in freewheeling mode also reduces the complexity of the test that may arise due to

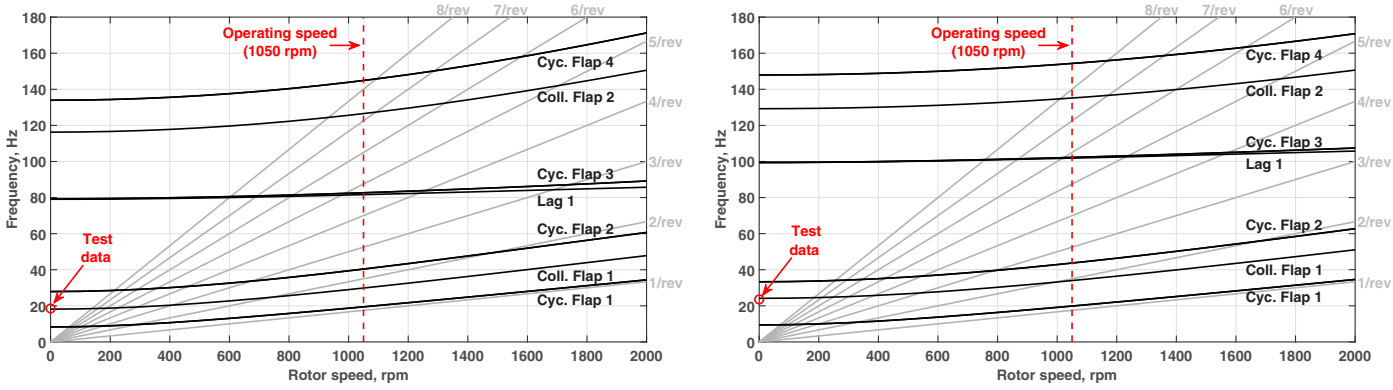

(a) Straight (b) Swept-tip

Fig. 7. Fanplot (coll.: collective mode, cyc.: cyclic mode; lines: predictions, symbols: test data).

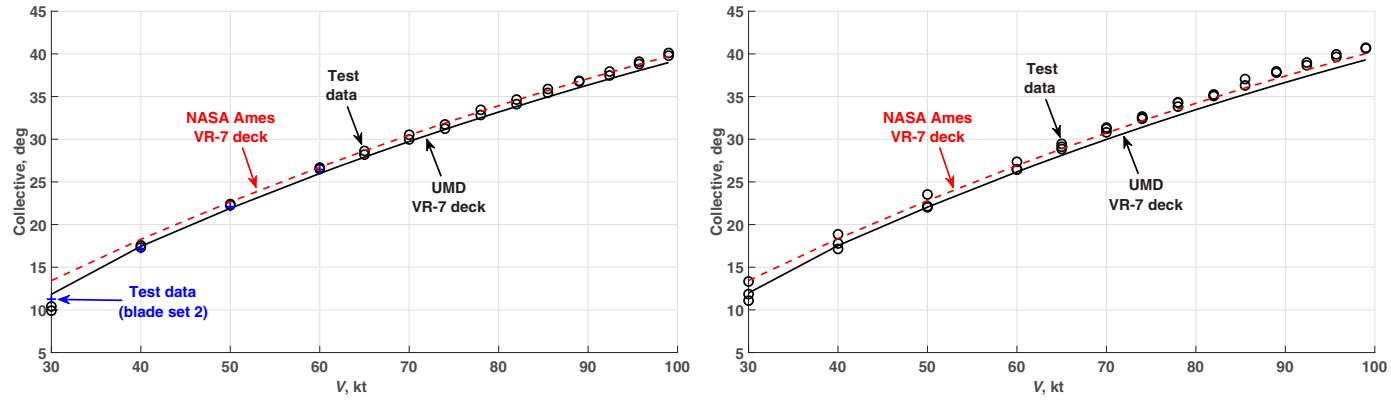

(a) Straight (b) Swept-tip

Fig. 8. Comparison of freewheeling collective predictions with wind tunnel test data at 1050 rpm (lines: predictions, symbols: test data).

powerplant stalling. Accurate prediction of the freewheeling collective is crucial as it has a direct effect on the coupling of rotor flap and lag modes. Figure 8 shows the change of freewheeling collective with respect to tunnel speed at 1050 rpm. The predictions are provided with UMD and NASA VR-7 airfoil decks. The two airfoil decks show different drag values at low angles of attack. Measurements with the two sets of straight blades are very close to each other, which signals consistency. Swept-tip blade collectives are slightly higher than straight blades. The predictions are satisfactorily close to the measurements, which validates the gross aerodynamic model.

Stability Predictions

The stability of the rotor/pylon/wing system can be calculated with two different methods. In the first method, the system is trimmed using Finite Element in Time (FET) and then numerical perturbation is applied to extract the mass, stiffness, and damping matrices due to the aerodynamic and inertial forces. Eigenvalues of the system then give the frequency and damping of the coupled system. A constant coefficient approximation is used in this method as it is valid and accurate for airplane mode axial flight. Stability roots are obtained in the fixed frame after applying a numerical multiblade coordinate transformation. In the second method, the system is again trimmed using FET but then the rotor controls are perturbed and the response is obtained with a time marching solution. This is a simulation of the test. The first method is computationally faster; however, only the transient response method can currently be used in UMARC-II for a gimballed hub. In this paper, gimbal-locked results were obtained with the first method (eigenvalue extraction) and gimbal-free results were obtained with the second method (transient response). The results with the two methods are identical for a gimbal-locked configuration.

Predictions were carried out for all the configurations shown in Table 6 and presented in Figs. 9–13 for each test run. Symbols show the test data, and lines show the predictions. Predictions were obtained up to 200 kt, which is the maximum speed of the Glenn L. Martin wind tunnel. Figure 9 shows comparison of wing beam (q_1) and wing chord (q_2) mode frequency predictions with the test data for the gimbal-free, freewheeling, wing fairings on configuration. The predictions align with the test data. The frequencies do not change with airspeed, and no interesting observation can be made. Frequency plots will therefore not be repeated for the other configurations.

Figures 10 and 11 show comparison of damping predictions with the test data for the gimbal-free, freewheeling, wing fairings on and off configurations. Good agreement is observed for the q_1 mode, especially for wing fairings on configuration (Fig. 10), but the test data are scattered at higher speeds. General trend of q_2 damping was captured for the wing fairings on configuration. A larger error is observed around 82 kt for wing fairings off, swept-tip configuration (Fig. 11(b)). No instability is observed at high speeds, though a slight decrease in chord damping is visible.

Figure 12 shows comparison of damping predictions with the test data for the gimbal-locked, freewheeling, wing fairings off configuration.

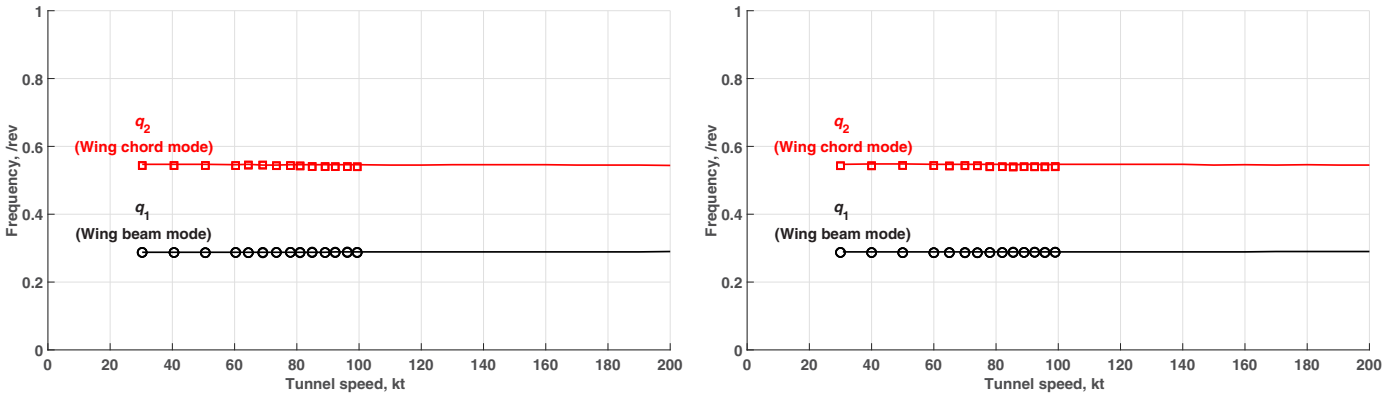

(a) Straight (b) Swept-tip

Fig. 9. Comparison of frequency predictions with wind tunnel test data for gimbal-free, freewheeling, wing fairings on configuration (lines: predictions, symbols: test data).

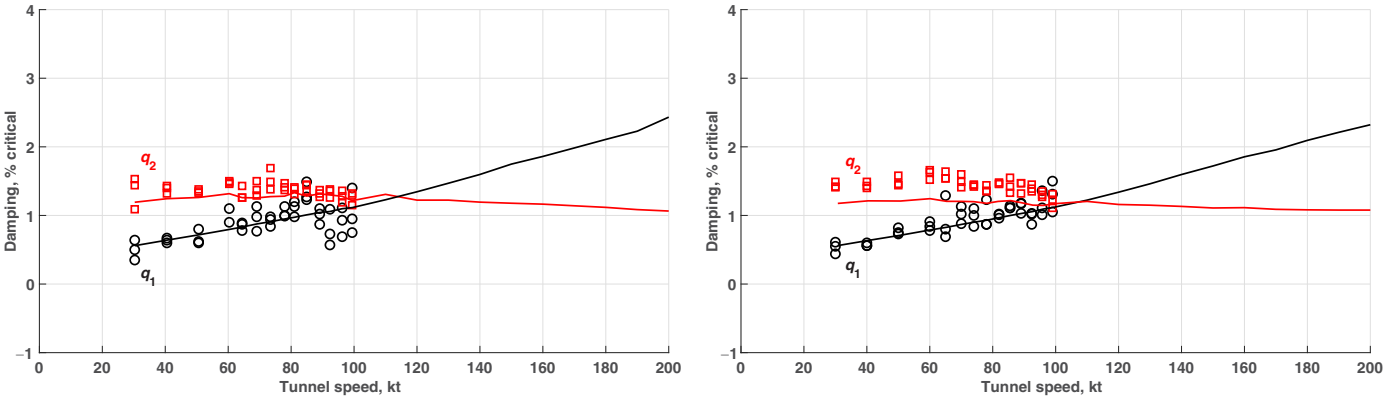

(a) Straight (b) Swept-tip

Fig. 10. Comparison of damping predictions with wind tunnel test data for gimbal-free, freewheeling, wing fairings on configuration (lines: predictions, symbols: test data).

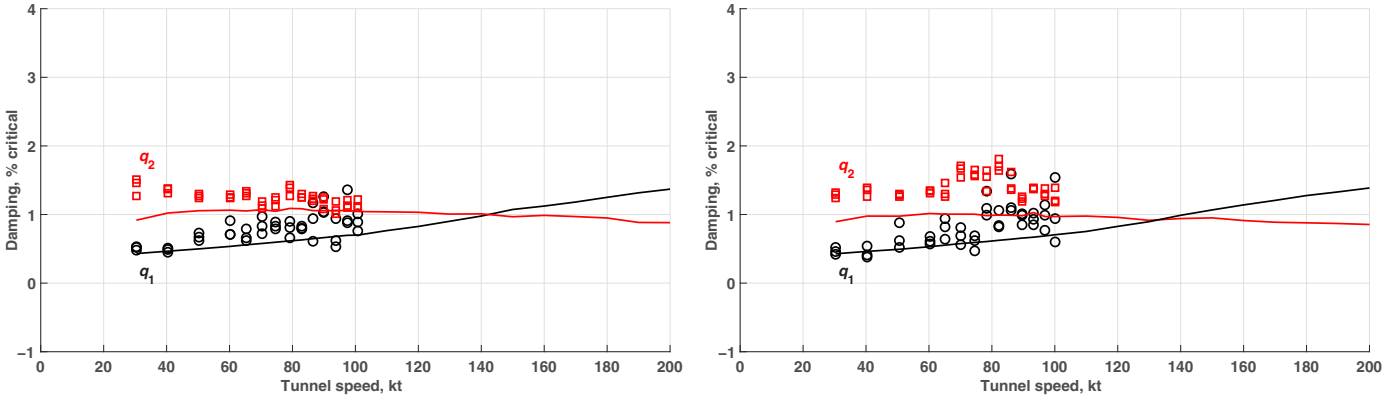

(a) Straight (b) Swept-tip

Fig. 11. Comparison of damping predictions with wind tunnel test data for gimbal-free, freewheeling, wing fairings off configuration (lines: predictions, symbols: test data).

Agreement for q_1 damping is satisfactory, but the test data are scattered for the swept-tip blades (Fig. 12(b)). The q_2 damping was predicted well for the straight blades at higher speeds but the trend at low speeds was not captured. On the other hand, q_2 damping for the swept-tip blades was underpredicted with an offset of around 0.9%, but the trend was captured.

Figure 13 shows comparison of damping predictions with the test data for the gimbal-locked, powered, wing fairings off configuration. Damping for q_1 was predicted accurately. The trend for q_2 damping for the straight blades was not captured up to 30 kt but predicted more accurately for the swept-tip blades. The maximum difference is about 0.8%.

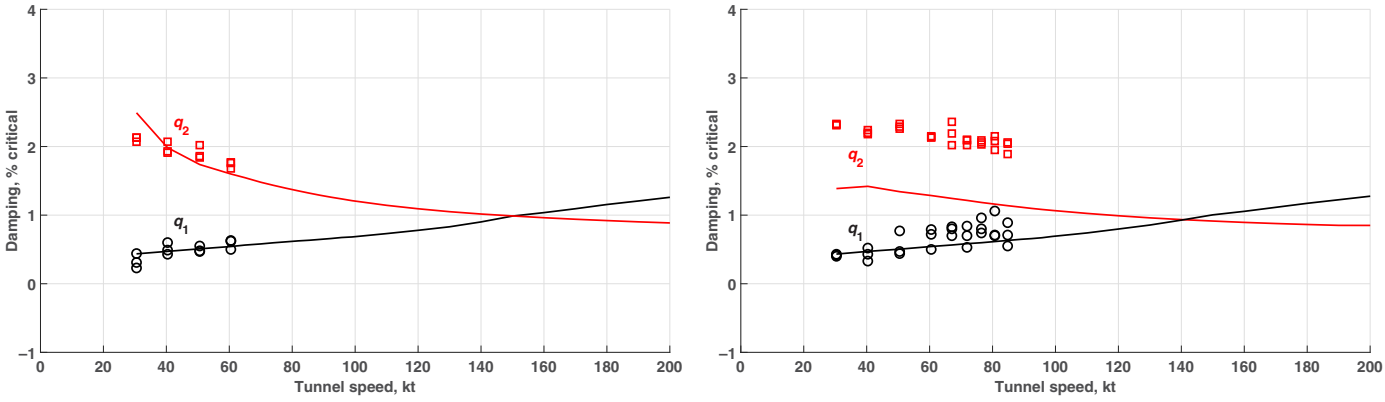

(a) Straight (b) Swept-tip

Fig. 12. Comparison of damping predictions with wind tunnel test data for gimbal-locked, freewheeling, wing fairings off configuration (lines: predictions, symbols: test data).

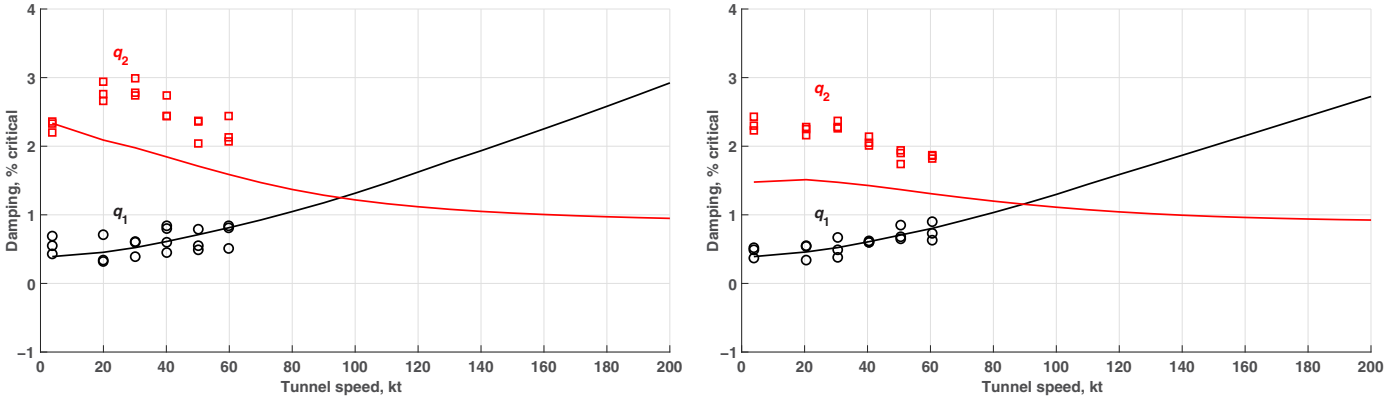

(a) Straight (b) Swept-tip

Fig. 13. Comparison of damping predictions with wind tunnel test data for gimbal-locked, powered, wing fairings off configuration (lines: predictions, symbols: test data).

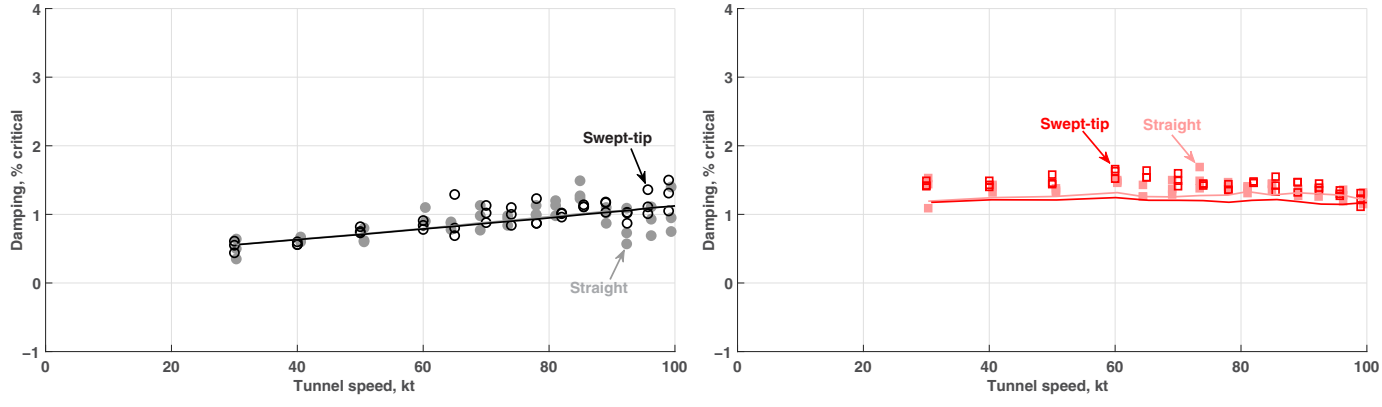

(a) Wing beam mode (b) Wing chord mode

Fig. 14. Comparison of straight and swept-tip blade damping test data for gimbal-free, freewheeling, wing fairings on configuration (lines: predictions, symbols: test data).

Comparison of Test Configurations

Figures 14–17 show comparison of the various test configurations together with the predictions for an assessment of impact of each parameter. The predictions are shown up to 100 kt to focus on the comparison.

Figure 14 compares the damping for straight and swept-tip blades for the gimbal-free, freewheeling, wing fairings on configuration. Both modes are slightly more damped at higher speeds with the swept-tip blades, but the scatter does not allow a clear conclusion. Figure 15 makes the same comparison for the gimbal-locked, freewheeling, wing fairings off

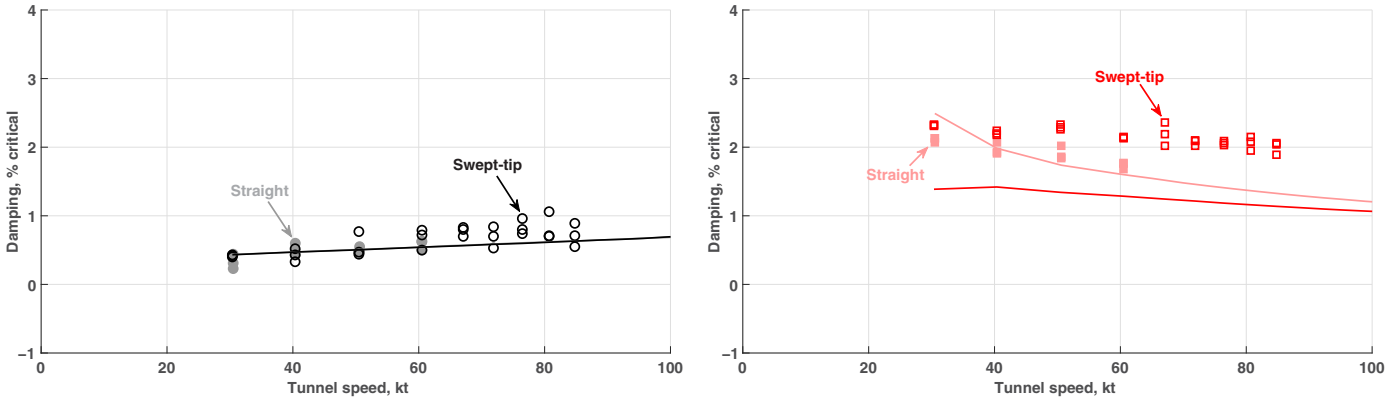

(a) Wing beam mode (b) Wing chord mode

Fig. 15. Comparison of straight and swept-tip blade damping test data for gimbal-locked, freewheeling, wing fairings off configuration (lines: predictions, symbols: test data).

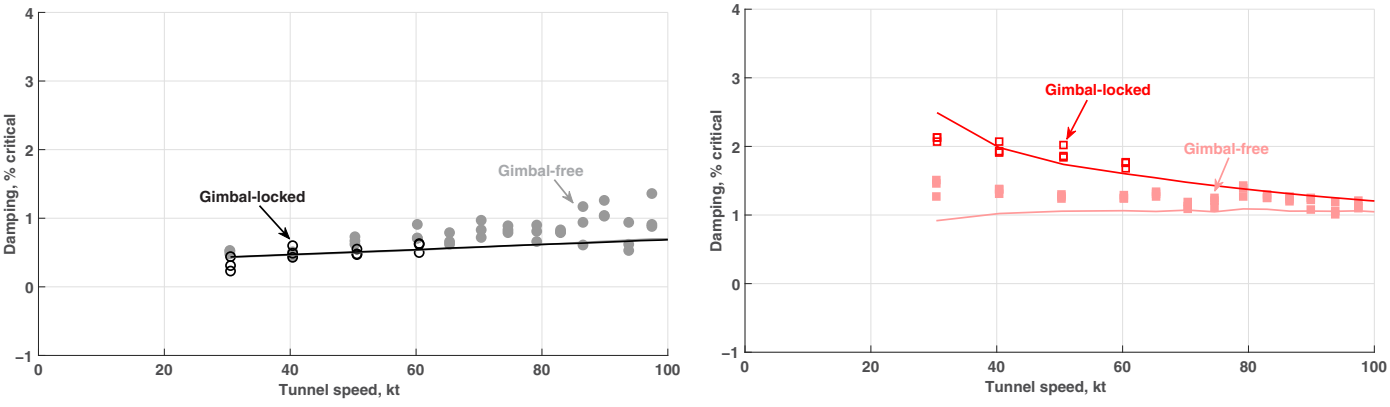

(a) Wing beam mode (b) Wing chord mode

Fig. 16. Comparison of gimbal-free and gimbal-locked damping test data for freewheeling, wing fairings off, straight blades configuration (lines: predictions, symbols: test data).

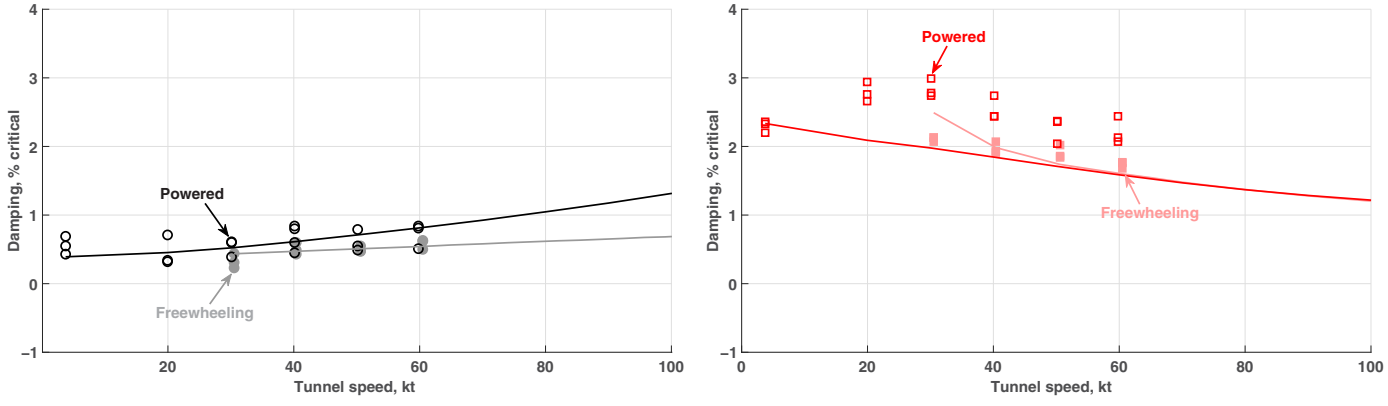

(a) Wing beam mode (b) Wing chord mode

Fig. 17. Comparison of freewheeling and powered mode damping test data for gimbal-locked, wing fairings off, straight blades configuration (lines: predictions, symbols: test data).

configuration. A clear increase in the q_2 test data is observed, which was not predicted by the analysis. The increase is about 0.4% at 60 kt. This is similar to the findings of Ref. 23 where q_2 is reported to be more sensitive to an aerodynamic center offset due to blade tip-sweep than q_1. Reference 2 makes a more detailed analysis of the current MTR swept-tip test data.

Figure 16 compares gimbal-free and gimbal-locked damping for the freewheeling, wing fairings off, straight blades configuration. The q_1 damping is slightly higher for the gimbal-free configuration, but the analysis predicts the same damping. Gimbal-locked shows about 0.5% higher damping for q_2, which was picked up by the analysis.

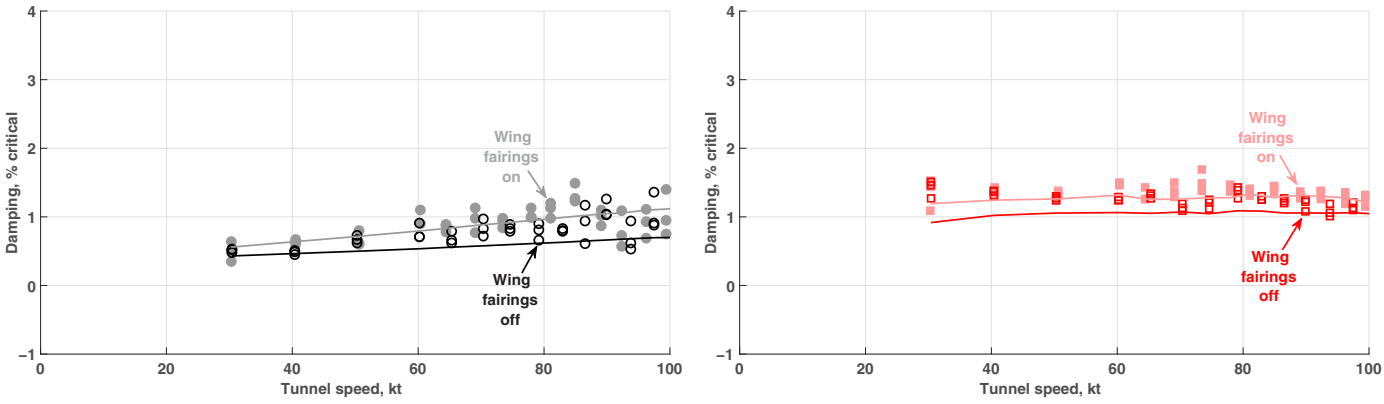

(a) Wing beam mode (b) Wing chord mode

Fig. 18. Comparison of wing fairings on and off damping test data for gimbal-free, freewheeling, straight blades configuration (lines: predictions, symbols: test data).

Figure 17 compares freewheeling and powered modes for the gimbal-locked, wing fairings off, straight blades configuration. Powered mode results in slightly higher damping for q_1 mode. The scatter in the data again prevents a definitive observation. The difference in the q_2 mode is more apparent; powered mode shows a peak around 30 kt and about 0.5% higher damping than freewheeling at higher speeds. Analysis did not predict this behavior.

Figure 18 compares wing fairings on and off damping for the gimbal-free, freewheeling, straight blades configuration. Analysis shows a distinct increase in q_1 damping at higher speeds when the wing fairings are on. Although not as clear due to the scatter, the test data also show this behavior. The increase in the q_2 test data is due to the higher structural damping when the wing fairings are installed (Table 4), not due to aerodynamics. The slightly different trends in the q_2 test data can be due to measurement errors.

Conclusions

University of Maryland's Maryland Tiltrotor Rig was tested in the Naval Surface Warfare Center Carderock Division 8-×10-ft subsonic wind tunnel. Frequency and damping data for wing beam and chord modes were collected up to 100 kt. Eight configurations were tested. These are gimbal-free and gimbal-locked, freewheeling and powered modes, wing fairings on and off, and straight and swept-tip blades. The test data for different configurations provided a rich source for fundamental understanding and analysis validation. The key conclusions are as follows:

1) Freewheeling predictions were validated for straight and swept-tip blades.

2) Wing beam damping was predicted accurately for all configurations.

3) Wing chord damping was generally underpredicted. The maximum difference is about 0.9%. The trends for the gimbal-locked, straight blades configurations (freewheeling and powered) were not captured.

4) No significant impact of swept-tip blades was observed for the gimbal-free configuration up to 100 kt.

5) Blade sweep increased wing chord damping for the gimbal-locked, freewheeling, wing fairings off configuration. The increase is about 0.4% at 60 kt. Analysis could not predict this increase.

6) Locking the gimbal provided about 0.5% higher damping for the wing chord mode, which was captured by the analysis.

7) Powered mode also resulted in 0.5% higher wing chord damping compared to freewheeling. Analysis could not predict this behavior.

8) Wing aerodynamics increased wing beam damping at higher speeds, although not as clearly as predictions due to the scatter in the data.

The test could only be conducted up to 100 kt due to tunnel safety restrictions. Future tests will explore speeds up to 200 kt, which will represent near 460-kt full-scale flight. Interesting parametric validation data are expected from these tests.

Acknowledgments

This work was carried out at the Alfred Gessow Rotorcraft Center, University of Maryland at College Park under the Army/Navy/NASA Vertical Lift Research Center of Excellence (VLRCOE) grant number W911W61120012 with technical monitoring from Mahendra Bhagwat and POCs Hyeonsoo Yeo (U.S. Army), Cecil Acree (NASA), and Wayne Johnson (NASA). We thank them for their valuable guidance on this work.

References

[1]Tsai, F., Sutherland, J., Akinwale, A., Morin, A., Gul, S., and Datta, A., "Whirl Flutter Test of the Maryland Tiltrotor Rig: Overview," Proceedings of the AIAA SciTech Forum, San Diego, CA and Virtual, January 3–7, 2022.

[2]Sutherland, J., Tsai, F., and Datta, A., "Whirl Flutter Test of the Maryland Tiltrotor Rig: Swept-tip Blades," Proceedings of the AIAA SciTech Forum, San Diego, CA and Virtual, January 3–7, 2022.

[3]Datta, A., Tsai, F., and Sutherland, J., "Design of a New Tilt Rotor Test Facility at the University of Maryland," Proceedings of the AIAA SciTech Forum, San Diego, CA, January 7–11, 2019.

[4]Tsai, F., Sutherland, J., and Datta A., "The Maryland Tiltrotor Rig (MTR): The Baseline Gimballed Hub," Proceedings of the 75th Annual Forum of the Vertical Flight Society, Philadelphia, PA, May 13–16, 2019.

[5]Gul, S., and Datta, A., "Design Analysis for a Mach-Scaled Hingeless Hub for the Maryland Tiltrotor Rig," 8th Asian/Australian Rotorcraft Forum Proceedings, Ankara, Turkey, October 30–November 2, 2019.

[6]Morin, A., "Fabrication, Wind Tunnel Testing, and Freewheeling Analysis of 4.75-ft Diameter Composite Tiltrotor Blades," Master's Thesis, University of Maryland, 2021, DOI: 10.13016/xniw-jyuc.

[7]Sutherland, J., and Datta, A., "Fabrication, Testing, and 3D Comprehensive Analysis of Swept-Tip Tiltrotor Blades," *Journal*

of the American Helicopter Society, **68**, 012002 (2023), DOI: 10.4050/JAHS.68.012002.

[8]Hall, W. E., Jr., "Prop-Rotor Stability at High Advance Ratios," *Journal of the American Helicopter Society*, Vol. 11, (2), April 1966, pp. 11–26, DOI: 10.4050/JAHS.11.2.11.

[9]Gaffey, T. M., "The Effect of Positive Pitch-flap Coupling (Negative δ_3) on Rotor Blade Motion Stability and Flapping," *Journal of the American Helicopter Society*, Vol. 14, (2), April 1969, pp. 49–67, DOI: 10.4050/JAHS.14.2.49.

[10]Johnson, W., "Dynamics of Tilting Proprotor Aircraft in Cruise Flight," NASA TN D 7677, 1974.

[11]Johnson, W., "Analytical Modeling Requirements for Tilting Proprotor Aircraft Dynamics," NASA TN D 8013, 1975.

[12]Johnson, W., Lau, B. H., and Bowles, J. V., "Calculated Performance, Stability, and Maneuverability of High-Speed Tilting-Prop-Rotor Aircraft," NASA TM 88349, 1986.

[13]Popelka, D., Sheffler, M., and Bilger, J., "Correlation of Test and Analysis for the 1/5-Scale V22 Aeroelastic Model," *Journal of the American Helicopter Society*, Vol. 32, (2), April 1987, pp. 21–33, DOI: 10.4050/JAHS.32.21.

[14]Barkai, S. M., and Rand, O., "The Influence of Composite Induced Couplings on Tiltrotor Whirl Flutter Stability," *Journal of the American Helicopter Society*, Vol. 43, (2), April 1998, pp. 133–145, DOI: 10.4050/JAHS.43.133.

[15]Srinivas, V., Chopra, I., and Nixon, M. W., "Aeroelastic Analysis of Advanced Geometry Tiltrotor Aircraft," *Journal of the American Helicopter Society*, Vol. 43, (3), July 1998, pp. 212–221, DOI: 10.4050/JAHS.43.212.

[16]Srinivas, V., and Chopra, I., "Validation of a Comprehensive Aeroelastic Analysis for Tiltrotor Aircraft," *Journal of the American Helicopter Society*, Vol. 43, (4), October 1998, pp. 333–341, DOI: 10.4050/JAHS.43.333.

[17]Ghiringhelli, G. L., Masarati, P., and Mantegazza, P., "Multi-Body Analysis of the 1/5 Scale Wind Tunnel Model of the V-22 Tiltrotor," Proceedings of the 55th Annual Forum of the American Helicopter Society, Montreal, Canada, May 25–27, 1999.

[18]Corso, L. M., Popelka, D. A., and Nixon, M. W., "Design, Analysis, and Test of a Composite Tailored Tiltrotor Wing," *Journal of the American Helicopter Society*, Vol. 45, (3), July 2000, pp. 207–215, DOI: 10.4050/JAHS.45.207.

[19]Nixon, M. W., Piatak, D. J., Corso, L. M., and Popelka, D. A., "Aeroelastic Tailoring for Stability Augmentation and Performance Enhancements of Tiltrotor Aircraft," *Journal of the American Helicopter Society*, Vol. 45, (4), October 2000, pp. 270–279, DOI: 10.4050/JAHS.45.270.

[20]Piatak, D. J., Kvaternik, R. G., Nixon, M. W., Langston C. W., Singleton, J. D., Bennett, R. L., and Brown, R. K., "A Parametric Investigation of Whirl-Flutter Stability on the WRATS Tiltrotor Model," *Journal of the American Helicopter Society*, Vol. 47, (2), April 2002, pp. 134–144, DOI: 10.4050/JAHS.47.134.

[21]Kvaternik, R. G., Piatak, D. J., Nixon, M. W., Langston, C. W., Singleton, J. D., Bennett, R. L., and Brown, R. K., "An Experimental Evaluation of Generalized Predictive Control for Tiltrotor Aeroelastic Stability Augmentation in Airplane Mode of Flight," *Journal of the American Helicopter Society*, Vol. 47, (3), July 2002, pp. 198–208, DOI: 10.4050/JAHS.47.198.

[22]Nixon, M. W., Langston, C. W., Singleton, J. D., Piatak, D. J., Kvaternik, R. G., Corso, L. M., and Brown, R., "Aeroelastic Stability of a Four-Bladed Semi-Articulated Soft-Inplane Tiltrotor Model," Proceedings of the 59th Annual Forum of the American Helicopter Society, Phoneix, AZ, May 6–8, 2003.

[23]Acree, C. W., Jr., Peyran, R. J., and Johnson, W., "Rotor Design Options for Improving Tiltrotor WhirlFlutter Stability Margins," *Journal of the American Helicopter Society*, Vol. 46, (2), April 2001, pp. 87–95, DOI: 10.4050/JAHS.46.87.

[24]Acree, C. W., Jr., "Effects of V-22 Blade Modifications on Whirl Flutter and Loads," *Journal of the American Helicopter Society*, Vol. 50, (3), July 2005, pp. 269–278, DOI: 10.4050/1.3092863.

[25]Yeo, H., Bosworth, J., Acree, C. W., Jr., and Kreshock, A. R., "Comparison of CAMRAD II and RCAS Predictions of Tiltrotor Aeroelastic Stability," *Journal of the American Helicopter Society*, **63**, 022001 (2018), DOI: 10.4050/JAHS.63.022001.

[26]Kreshock, A. R., Thornburgh, R. P., and Yeo, H., "Comparison of Comprehensive Analyses Predicting Whirl Flutter Stability of the Wing and Rotor Aeroelastic Test System," *Journal of the American Helicopter Society*, **64**, 042010 (2019), DOI: 10.4050/JAHS.64.042010.

[27]Yeo, H., and Kreshock, A. R., "Whirl Flutter Investigation of Hingeless Proprotors," *Journal of Aircraft*, Vol. 57, (4), July 2020, pp. 586–596, DOI: 10.2514/1.C035609.

[28]Kreshock, A. R., Thornburgh, R. P., Kang, H., Yeo, H., Shen, J., and Baggett, J., "Pretest Flutter Predictions of the Upcoming Aeroelastic Tiltrotor Wind Tunnel Test," Proceedings of the 76th Annual Forum of the Vertical Flight Society, Virtual, October 5–8, 2020.

[29]Yeo, H., Kang, H., and Kreshock, A. R., "Unified Modeling of the TiltRotor Aeroelastic Stability Testbed for Proprotor Whirl Flutter," *Journal of Aircraft*, Vol. 60, (3), May 2023, pp. 857–869, DOI: 10.2514/1.C036950.

[30]Gul, S., and Datta, A., "Aeroelastic Loads and Stability of Swept-Tip Hingeless Tiltrotors toward High-Speed Instability-Free Cruise," *Journal of the American Helicopter Society*, **68**, 012001 (2023), DOI: 10.4050/JAHS.68.012001.

[31]Bir, G., and Chopra, I., "Development of UMARC (University of Maryland Advanced Rotorcraft Code)," Proceedings of the American Helicopter Society 46th Annual Forum, Washington, DC, May 21–23, 1990.

[32]Gul, S., and Datta, A., "Development of an Aeromechanics Solver for Loads and Stability of Hingeless Tiltrotors," *Journal of Aircraft*, Vol. 60, (1), January 2023, pp. 143–159, DOI: 10.2514/1.C036944.

[33]Hodges, D. H., and Dowell, E. H., "Nonlinear Equations of Motion for the Elastic Bending and Torsion of Twisted Nonuniform Rotor Blades," NASA-TN-D-7818, 1974.

[34]Tasker, F. A., and Chopra, I., "Assessment of Transient Analysis Techniques for Rotor Stability Testing," *Journal of the American Helicopter Society*, Vol. 35, (1), January 1990, pp. 39–50, DOI: 10.4050/JAHS.35.39.

[35]Kvaternik, R. G., "A Review of Some Tilt-Rotor Aeroelastic Research at NASA-Langley," *Journal of Aircraft*, Vol. 13, (5), May 1976, pp. 357–363, DOI: 10.2514/3.44530.